Introduction to Aerial Robotics - A Robust Control Approach

Jiayao Wang and Vinzent Rudolf

Abstract— **In this paper a control approach for a multirotor aerial vehicle (MAV) is presented. The goal is to implement a robust feedback controller, which compensates poor knowledge about multiple parameters of the model as well as noise on feedback signals and external disturbances. The paper starts with an introduction to the theory used to achieve a robust controller, mainly the theory about the DK-synthesis and the method to show how robustness is guaranteed. For the design of the controller uncertainties and disturbances are implemented and justified. Finally a comparison between the results of the designed robust controller (RC) and the near-hovering-controller (NHC) treated in the lecture "Introduction to aerial robotics" is drawn. Additionally, the behavior of the controlled system is discussed, and how the controller meets the performance requirements.**

I. THEORETICAL BACKGROUND

The theory of robust control is well known for linear time invariant systems. This chapter gives the most important theoretical results and a guideline to use these results. A mathematical model is always an abstraction of the reality. This results in a mismatch between model and the real system, which is called *uncertainty*. The goal of robust control is to handle uncertainties in a systematic fashion when designing a controller for the system.

A. The General Framework

Uncertainty is a very general expression: It can vary from *simple* parameter variations to complete unknown *system dynamics*. Hence in the beginning a general framework to handle different types of uncertainties is introduced. The general open-loop interconnection called P includes following signals, which are needed for the closed loop with uncertainties Δ and controller K

- z_Δ denotes the inputs of the uncertainties (input of Δ)
- ω_Δ denotes the outputs of the uncertainties (output of Δ)
- ω denotes the signals that affect the system and cannot be influenced by the controller (e.g. disturbances, reference)
- z denotes the performance channels (e.g. error)
- u denotes the control input (output of K)
- y denotes input signals for the controller (input of K)

By defining this general framework, the closed-loop interconnection can easily be determined. The closed-loop interconnection is computed by a lower or upper linear fractional transformation (LFT). It is also called star product.

$$P \star K = P_{11} + P_{12}K(I - P_{22}K)^{-1}P_{21}$$
$$\Delta \star P = P_{22} + P_{21}\Delta(I - P_{11}\Delta)^{-1}P_{12} \quad (1)$$

whereby the respective matrices $P_{(\cdot,\cdot)}$ are chosen properly so that dimensions fit. The *Robust Control Toolbox* offers a very simple approach in order to handle uncertainties. Uncertainties must be defined corresponding to its type (*ureal* to define just a real valued uncertainty, *ucomplex* to define a complex-valued uncertainty, or *usys* to define a dynamic uncertainty). Afterwards the system can easily be build up according to its interconnections. It is recommended to use the command *sysic* to easily build state-space realization even for complicated (closed-loop) interconnections. The resulting system is an uncertain system object. With the command *lftdata* one can easily pick out the corresponding open-loop interconnection. Furthermore, using the command *usubs* one

can create one particular system (*usample* generates randomly chosen samples). However, so that the introduced tools work, the set of all uncertainties Δ must be star-shaped with center 0.

B. Theoretical Guarantees

As mentioned above, the closed-loop interconnection can be calculated by the star product. Therefore, following abbreviation is introduced to highlight M

$$P \star K = N = \begin{pmatrix} M & N_{12} \\ N_{21} & N_{22} \end{pmatrix}$$

Hence, the closed-loop interconnection of N and Δ is given by

$$\Delta \star N = N_{22} + N_{21}\Delta(I - M\Delta)^{-1}N_{12}$$

Starting from this representation, following theorem can be proved

Theorem 1: Suppose M is a proper and stable transfer matrix. If

$$\det(I - M(i\omega)\Delta) \neq 0 \quad \forall \Delta \in \boldsymbol{\Delta}, \ \omega \in \mathbb{R} \cup \{\infty\}$$

then

$I - M\Delta$ has a proper and stable inverse for all $\Delta \in \boldsymbol{\Delta}$ [3]. The major advantage of this theorem is, that it suffices to check only the imaginary axes for stability, and not the full right-half plane. Thereby, the problem is turned into a simpler problem of linear algebra [3], which can be solved very efficiently and is able to take the structure of Δ into account.

The famous *Structured Singular Value* (SSV) is a simple test for theorem 1. It evaluates M and Δ at specific frequencies. Fortunately, one can calculate a *lower* and *upper* bound for the SSV pretty efficiently [3]. The lower bound indicates robust stability for the closed-loop for all $\|\Delta\|_\infty < \frac{1}{\gamma_l}$. On the other side, the upper bound implies that there exists a destabilizing uncertainty with $\|\Delta\|_\infty < \frac{1}{\gamma_u}$ [4]. Obviously, these bounds pushes Δ below the level $\frac{1}{\gamma}$ for all frequencies. This is not always desired, because from a practical point of view, dynamic uncertainties have different gains at different frequencies. Hence uncertainty weights W_Δ are used to normalize the input and output of Δ. Additionally, if Δ only consists of fully uncertain blocks, than the SSV tests coincides with the Small-Gain theorem.

If K stabilizes P, it achieves nominal performance if $\|N_{22}\|_\infty \leq 1$. K achieves robust performance if

$$(I - M\Delta)^{-1} \text{ is proper and stable, and } \|\Delta \star N\|_\infty \leq \gamma$$

holds for all $\Delta \in \boldsymbol{\Delta}$ with $\|\Delta\|_\infty \leq \frac{1}{\gamma}$. Furthermore, it can be shown, that an additional SSV test can be used to check robust performance. This theorem is known as the *Main Loop Theorem* as presented in [3].

C. H_∞ and DK Synthesis

After presenting the main theory of robust control, this subsection will focus more on the controller design. The nominal controller for P is minimizing the H_∞-norm of $P \star K$.

$$\min_K \quad \|P \star K\|_\infty$$
$$\text{s.t.} \quad K \text{ stabilizes } P \quad (2)$$

Suppose $\|P \star K\|_\infty \leq \gamma$. This means that the gain of the closed-loop is pushed below the level γ for all frequencies. This is in general not desired, rather user-defined shapes are more useful. This is obtained through the use of performance weights W_P (similar to uncertainty weights). The adapted plant is called $\tilde{P}$. Unfortunately, the H_∞ problem does not take uncertainties into account. Hence the so called *DK-Synthesis* is used. This approach uses so-called *D-Scalings* in the controller design. These scalings are used to compute better upper bounds of the SSV test. However, it can not be proven, that this scheme leads to an optimal controller. Nevertheless, it turned out to be pretty successful in practical applications [3]. The MATLAB command is *dksyn*.

II. System Dynamics

The system dynamic equations for a MAV are derived under the assumption that the MAV is a rigid body system. Hence, the MAV can be simplified as a mass point in its center of gravity p. The individual thrusts of all rotors are summarized in the input vector

$$u = \begin{pmatrix} u_T & \tau_x & \tau_y & \tau_z \end{pmatrix}^T \in \mathbb{R}^4$$

Thereby u_T is the effective thrust in the z-direction of the body coordinate system and τ are the individual torques around the three body axes. Hence, the complete dynamics of a MAV are given by

$$\dot{x} = \begin{pmatrix} \dot{p} \\ \ddot{p} \\ \dot{\eta} \\ \dot{\omega} \end{pmatrix} = \begin{pmatrix} \dot{p} \\ ge_z \\ T(\eta)\omega \\ -J_B^{-1}[\omega]_\wedge J_B \omega \end{pmatrix} + \begin{pmatrix} 0 \\ -\frac{1}{m}R(\eta)e_z u_T \\ 0 \\ J_B^{-1}\tau \end{pmatrix} \quad (3)$$

as follows from [6]. Obviously, the dynamics are nonlinear. Therefore, the problem to design a robust controller for (3) is splitted up into different sub tasks

1) decouple dynamics of (3) into altitude and attitude dynamics
2) design robust controller for altitude and attitude independently from each other
3) design cascaded position controller for x and y

Hence, the system dynamics are reformulated to equations (4) and (5). Block diagrams of the reformulated system dynamics are added to the appendix (see figure 7 and 8). The gravity vector g is used as additional input to the system. However, it is known to the controller. In general, g can be interpreted as an external force, which is measurable. The approximated system contains following simplifications and extensions

1) The difference between commanded torques / thrusts and applied torques / thrusts is covered by dynamic and parametric uncertainties.
2) Uncertainties for nonlinear terms are introduced.
3) All measurements are noisy.
4) External torques and external forces can also occur as inputs.

The next sections will deal with those extensions. In the end, the cascaded x and y position controller is introduced.

A. Actuator Uncertainties

The altitude dynamics consist of a real parametric uncertainty Δ_m, which describes a non-dynamic relative mass deviation $\frac{\hat{m}-m}{\hat{m}}$ (see equation (6)). Thereby, it is assumed that the nominal mass m does not differ more than 10% from the real (actual / uncertain) mass $\hat{m}$. That is, in the case of a manned multi-copter, the difference of weight of different pilots, in delivery drones the weight of the parcel being delivered or

additional equipment added to a research MAV. Therefore, $W_m = 0.1$ is chosen.

$$\frac{1}{\hat{m}} = \frac{1}{m}(1 + W_m \Delta_m) \quad \Leftrightarrow \quad W_m \Delta_m = \frac{\hat{m} - m}{\hat{m}} \quad (6)$$

In the dynamics a direct feedthrough of the desired thrust u_T is assumed. However, the motors have internal dynamics. Additionally, in practice, the desired torque can not be applied exactly. Both neglects are covered by the uncertainty $W_{u_T}\Delta_{u_T}$ (see equation (7)). The motor dynamics are designed as PT1 filter with a maximum time constant of $T = 10$ms. The gain k describes a fixed relation between desired and actual torque, which can be compared to a tilting of the characteristic curve of the motor. Here a maximum tilting of $|k| < 0.5$ is assumed.

$$G = \frac{1 + k}{Ts + 1} = 1 + W_{u_T}\Delta_{u_T} \quad \Leftrightarrow \quad W_{u_T}\Delta_{u_T} = \frac{k - Ts}{Ts + 1} \quad (7)$$

In figure 1 different resulting motor uncertainties are visualized. For small frequencies, the damping of the commanded torque depends only on the gain k. However, for larger frequencies no torque is applied, because the motor is too slow. The torques of the attitude dynamics consist of the same motor uncertainty structure (7). Furthermore, the maximum time constant of each torque is $T = 40$ms, because multiple motors have to create thrust, so that a torque around the body axes is applied. The constant gain is chosen as $k = 0.5$, as mentioned before. Uncertainties of the inertia are not covered explicitly. Nevertheless, due to the factor $J_B^{-1}\tau$ possible deviations are already covered by the torque uncertainties.

B. Nonlinear Terms

Because Robust Control Theory can only be applied to linear systems, the system dynamics (3) have to be brought into a linear form. The nonlinear terms are $R(\eta)$, $T(\eta)$ and $[\omega]_\wedge J_B \omega$. In order to not simply ignore these terms, they are introduced as uncertain systems into the uncertain system dynamics (4):

1) $R(\eta)$: For $R(\eta)$ no additional uncertainty object is introduced. The uncertainty of this term is already implicitly captured with Δ_m and Δ_{u_T}.

2) $T(\eta)$: The term $T(\eta)$ is approximated by the uncertainty $\Delta_{T(\eta)}$. Therefore, $T(\eta)$ is linearized around $\begin{pmatrix} \phi & \theta \end{pmatrix} = \begin{pmatrix} 0 & 0 \end{pmatrix}$. The new linearized variables $\Delta\phi$ and $\Delta\theta$ are used as dynamic uncertainties Δ_ϕ and Δ_θ. A maximum roll and pitch angle of $|\phi|, |\theta| < 10°$ is assumed. The $10°$ is used as output weight W_η. Hence, $\Delta_{T(\eta)}$ is given by

$$\begin{aligned} \Delta_{T(\eta)} &= T(\eta)\big|_{\phi,\theta=0} + \frac{\partial T(\eta)}{\partial(\phi,\theta)}\bigg|_{\phi,\theta=0} \begin{pmatrix} W_\eta \Delta_\phi \\ W_\eta \Delta_\theta \end{pmatrix} \\ &= \begin{pmatrix} 1 & 0 & W_\eta \Delta_\theta \\ 0 & 1 & -W_\eta \Delta_\phi \\ 0 & W_\eta \Delta_\phi & 1 \end{pmatrix} \end{aligned} \quad (8)$$

3) $[\omega]_\wedge J_B \omega$: The inertia matrix J_B is assumed to have only entries on the main diagonal, whereby $J_{xx} \equiv J_{yy}$. Therefore, the term $[\omega]_\wedge J_B \omega$ results in the following

$$\begin{aligned} [\omega]_\wedge J_B \omega &= \begin{pmatrix} (J_{zz} - J_{yy})\omega_z\omega_y \\ (J_{xx} - J_{zz})\omega_z\omega_x \\ 0 \end{pmatrix} \\ &= \begin{pmatrix} 0 & (J_{zz} - J_{yy})W_{\omega_z}\Delta_{\omega_z} & 0 \\ (J_{xx} - J_{zz})W_{\omega_z}\Delta_{\omega_z} & 0 & 0 \\ 0 & 0 & 0 \end{pmatrix} \omega \\ &= \Delta_{[\omega]_\wedge J_B}\omega \end{aligned} \quad (9)$$

Obviously, the nonlinear term can be rearranged, so that the inner matrix only depends on ω_z. Therefore, this term is exchanged with a dynamic uncertainty Δ_{ω_z}. This uncertainty

$$\dot{x} = \begin{pmatrix} \dot{p}_z \\ \ddot{p}_z \\ \dot{\eta} \\ \dot{\omega} \end{pmatrix} = \begin{pmatrix} 1 & 0 & 0 & 0 \\ 0 & 0 & 0 & 0 \\ 0 & 0 & 0 & \Delta_{T(\eta)} \\ 0 & 0 & 0 & -J_B^{-1}\Delta_{[\omega]_\wedge}J_B \end{pmatrix} \begin{pmatrix} p_z \\ \dot{p}_z \\ \eta \\ \omega \end{pmatrix}$$

$$+ \begin{pmatrix} 0 & 0 & 0 & 0 & 0 \\ -\frac{1}{m}(1+W_m\Delta_m)(1+W_{u_T}\Delta_{u_T}) & -\frac{1}{m} & 1 & 0 & 0 \\ 0 & 0 & 0 & 0 & 0 \\ 0 & 0 & 0 & J_B^{-1}(1+W_\tau\Delta_\tau) & J_B^{-1} \end{pmatrix} \begin{pmatrix} u_T \\ f_{Ext} \\ g \\ \tau \\ \tau_{Ext} \end{pmatrix} \tag{4}$$

$$\tilde{x} = \begin{pmatrix} \tilde{p}_z \\ \dot{\tilde{p}}_z \\ \tilde{\eta} \\ \tilde{\omega} \end{pmatrix} = \begin{pmatrix} p_z \\ \dot{p}_z \\ \eta \\ \omega \end{pmatrix} + \begin{pmatrix} n_z \\ n_{\dot{z}} \\ n_\eta \\ n_\omega \end{pmatrix} \tag{5}$$
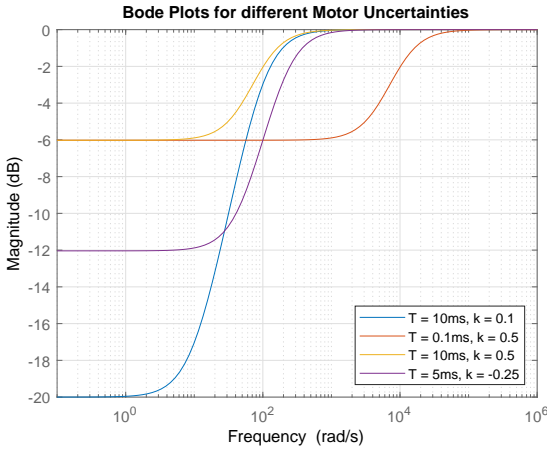

Fig. 1. Motor Uncertainties

has an output weight $W_{\omega_z} = \frac{2}{s+1}$. The 2 is the assumed maximum body rate $|\omega_z| < 2$. A PT1 filter is used to describe the correlation between ω_z and $\omega_{x,y}$: only greater ω_z occur, if the other body rate has less dynamics $\Rightarrow$ two body rates do not change simultaneously very fast.

All dynamic uncertainties of the nonlinear terms are very unspecific, so that nearly any possible (stable) transfer function could be obtained by them. This approach has the advantage that all possible situations are covered under the assumption that the maximum values fit. However, these uncertainties are in general time variant, because the exact transfer function depends on the current state vector x. This time variant behavior is formally not covered in Robust Control Theory. Nevertheless, simulation shows satisfactory results.

C. Noisy Measurements

In real world systems a main problem in the control feedback is the noise layered on top of the feedback signal. To create a system simulation close to real world applications noise is added to the feedback channels of p_z, $p_{\dot{z}}$, Euler-angles η and body rates ω (see equation (5)). This is taken into account in the controller design by introducing additional performance channels from input noise to controller error. Accuracy values for p_z, $\dot{p}_z$ and the heading are taken from the datasheet of a GNSS receiver [5]. As simplification the yaw angle is assumed to be the heading angle. The accuracy values are given by

$$|n_z| < 2m, \quad |n_{\dot{z}}| < 0.5\frac{m}{s}, \quad |n_\psi| < 0.3°$$

Due to missing data, the accuracy of ϕ and θ is estimated as $0.5°$. The noise of each channel is sampled from a uniform

distribution using the before mentioned values as bounds. The variance of the normal distributed noise n_ω is taken from the datasheet [1] ($\sigma_{n_\omega} = 0.07\frac{rad}{s}$). The measurement is called $\tilde{x}$.

D. External Inputs

Two additional input channels are added into the system structure to take external forces and external torques like those created by wind, into account. For simulation purposes following external inputs are assumed

$$f_{Ext} = 1 \cdot \sin(1t), \quad \tau_{Ext} = 1 \cdot \sin(0.1t)$$

These assumptions hold true in a test scenario with little wind or moving air masses or in a laboratory, where external forces are applied to either the center of mass or to the extended body.

E. Position Controller for x and y

It is assumed, that the MAV is in a state in which almost all Euler-angles are close to zero. Therefore the altitude and the rotation can be controlled separately. The position controller for x and y is implemented in the same way as for the near hovering controller. Unfortunately, it is not possible to apply the robust control theory to this structure. This paper, deals only with applying robust control theory to altitude and attitude dynamics. Nevertheless, a possible extension is proposed: The desired and actual x and y position have to be rotated using the current yaw angle. A noise on the yaw angle is later used as additional input channel. The linearization of the last column of the rotation matrix R around $\begin{pmatrix} \phi & \theta & \psi \end{pmatrix} = \begin{pmatrix} 0 & 0 & 0 \end{pmatrix}$ leads to the following expression

$$R_{lin} = R(\eta)e_z\big|_{\eta=0} + \frac{\partial R(\eta)e_z}{\partial(\phi,\theta,\psi)}\bigg|_{\eta=0} \eta = \begin{pmatrix} \theta \\ -\phi \\ 1 \end{pmatrix} \tag{10}$$

Hence, the inputs to $\ddot{x}$ and $\ddot{y}$ are θu_T and $-\phi u_T$. Afterwards u_T is splitted into a nominal part for $\dot{z} = 0$ and an uncertain dynamic part:

$$u_T := u_{T_{nom}} + W_{u_{T_{x,y}}}\Delta_{u_{T_{x,y}}}$$

Therefore, the horizontal position dynamics rotated by the yaw angle are given by

$$\dot{x} = \begin{pmatrix} \dot{p}_x \\ \ddot{p}_x \\ \dot{p}_y \\ \ddot{p}_y \end{pmatrix} = \begin{pmatrix} \dot{p}_x \\ 0 \\ \dot{p}_y \\ 0 \end{pmatrix} - \frac{1}{m}(u_{T_{nom}} + W_{u_{T_{x,y}}}\Delta_{u_{T_{x,y}}}) \begin{pmatrix} 0 \\ \theta \\ 0 \\ -\phi \end{pmatrix}$$

Afterwards these dynamics are combined with the attitude dynamics. In the end, a controller is designed to follow a desired position. This will end up in a cascaded structure. The performance weight $W_{u_{T_{x,y}}}$ is supposed to be similar to a PT1-filter: high dynamics on θ or ϕ do not have an influence on the position. Unfortunately, it is not possible to further investigate this idea in this paper. As mentioned above, the cascaded structure from the near hovering controller has been used for further analysis. The overall control structure is visualized in figure 2.
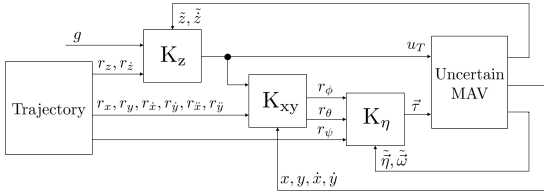
Fig. 2. Sketch of the robust control loop

III. PROGRESSION AND IMPLEMENTATION

A robust controller was achieved by starting with a very simplified model of the MAV and augmenting the controller in an iterative process. In this section three main steps in the progression to the final controller are further elaborated. The process is started with the very simple first model and the proof of concept, which is augmented with first simple uncertainties and the controller for those. In the end further uncertainties are implemented as well as the ability for trajectory flight.

A. First model and main idea

The main idea of the control approach is creating a controlled system with uncertainties, which then gets transferred into a P-Δ-structure with the $sysic$ and lft command. This structure can then be controlled by separately designed controllers in the P-Δ-K-structure for the altitude, see figure 3, and the P-Δ-K-structure for the attitude, see figure 4. As a first test a simple model of the MAV is implemented. It has only the z-axis as a degree of freedom and only an input u_T. Implementing a first controller, obtained through the $dksyn$ command, together with a simple real mass uncertainty and the gravitational disturbance g, delivers promising results. This means the controller is able to follow an altitude trajectory and to stabilize the system. In the next step the complete model for the system as shown in equation (4) is implemented and connected to the previously generated altitude controller as well as with a newly designed attitude controller. In combination with the position controller from [6] and a trajectory generation block, this leads to the control structure shown in figure 2.
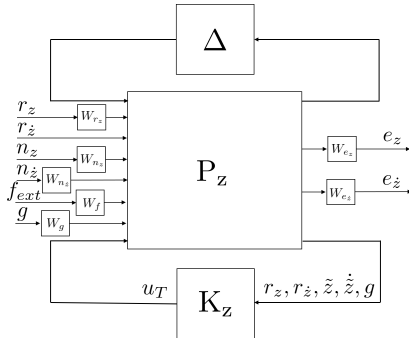

Fig. 3. Δ-P-K structure for altitude control

B. Separate design of altitude and attitude controller

The design of the two different controllers relies strongly on the implemented uncertainties and the added external influences. The altitude controller remained similar to the first approach, with the addition of a separate performance channel for the velocity $\dot{p}_z$ and the before introduced dynamic uncertainty for the thrust u_T given by the controller.

The attitude controller deals with the rotational dynamics of equation (4) and an dynamic uncertainty in the torque output τ of the controller. Another uncertainty of the attitude dynamics is the linearization of the rotational dynamics, which is added as a multiplication uncertainty to the system.
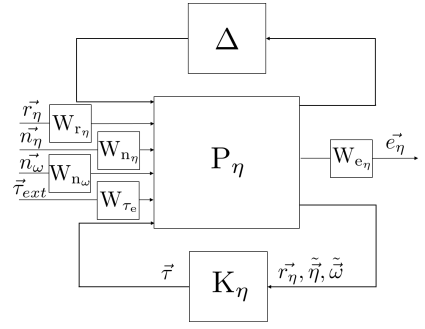

Fig. 4. Δ-P-K structure for attitude control

C. Trajectory Generation

To actually fly with this controller, a trajectory generator is implemented. Its inputs are the setpoints of the trajectory and its output is a two times differentiable curve for position p_{des}, a one time differentiable desired path for velocity $\dot{p}_{des}$ and a continuous curve for the acceleration $\ddot{p}_{des}$. With T being the time to fly from one setpoint p_i to the next setpoint p_{i+1} and t being the time passed between those, the curve for the position results from

$$p_{des}(t) = p_i + (p_{i+1} - p_i) \sum_{k=n+1}^{2n+1} a_k \left(\frac{t}{T} \right)^k. \quad (11)$$

The parameters a_k make sure that all derivatives of the trajectory are equal to zero at $t = 0$ and $t = T$. The parameters are given by $a_0 = 10$, $a_1 = -15$ and $a_2 = 6$. This trajectory generation is based on [2]. The desired yaw is calculated by

$$\psi_{des} = \arctan \left(\frac{\dot{p}_y}{\dot{p}_x} \right) \quad (12)$$

so that the MAV points into the direction of flight.

IV. RESULTS

In this section the results of the designed robust controller are analyzed. In the beginning the controller structure is introduced. Afterwards a closer look regarding performance and stability is done. In the end, a simulation study is carried out for comparing NHC and RC. The final robust controllers are each a LTI system with following properties:

1) The altitude controller consists of 16 states, 5 inputs (g, p_{des_z}, $\dot{p}_{des_z}$, $\tilde{p}_z$, $\dot{\tilde{p}}_z$) and 1 output (thrust u_T).
2) The attitude controller has got 35 states, 9 inputs (r_η, $\tilde{\eta}$, $\tilde{\omega}$) and 3 outputs (torques τ)

A. Robust Stability and Robust Performance

During the weight design it turns out, that the $dksyn$ command is able to compute better controllers, if different performance weights than the desired dynamic behavior are used. Therefore, the performance is not supposed to be analyzed with the design weights, instead additional *real-world* performance weights are used for performance analysis. However, this task has not been done, instead performance has only been analyzed during simulation studies. Nevertheless, robust performance analysis will give very good insights, how well actually all possible uncertain systems can fulfill the given requirements. As showed in figure 9 and 10 we analyze the robustness of channels from the desired trajectories, noises and external inputs to the tracking error in the frequency domain. In these bode diagrams the *weights* demonstrate the requirements in different performance channels. The *nominal* curves show frequency behaviors of the nominal systems with the robust controllers. For each channel we randomly sample 50 combinations of the uncertainties to test the robust performances

of the controllers, whose results are presented with the green lines. Overall it can be concluded that robustness is achieved satisfactory in the closed loop according to these bode plots. The altitude controller (figure 10) shows small error deviation at low frequencies and a small peak value around $90\frac{rad}{s}$ for the uncertain samples in the channel $r \to e(z)$, which means that the desired trajectory can be well tracked for slow dynamics. In the real world the measurement noise normally has high frequency, and in the bode plots of channels from measurement noises to position error we can see that the sampling of the uncertainties has very small gain at high frequency, i.e. the controller has good noise restrain performance. In contrast to noise, external forces occur at low frequencies, so we design the target weights like low-pass filters for the channels *external inputs to error* as showed in the figures. All of the sampled uncertainties can fulfill that. In the gravitational channel the magnitude keeps a small value for all frequencies, which is in accordance with our expectation. Similar to the altitude controller, the bode diagrams in figure 10 also prove good robust performance of the attitude controller with exception for the channel from external torques to tracking errors of Euler angles, in which a peak value close to 1 occurs around $10\frac{rad}{s}$. Nevertheless, the controller can reduce the effect of external torques at low frequencies as well.

Furthermore, robust stability does not depend on the weights of the performance channels. Stability of linear systems does not depend on the inputs (in contrast to nonlinear systems). Therefore, it is possible to give stability margins $r = \frac{1}{\gamma}$ (see figure 5). The attitude controller is stable for all possible

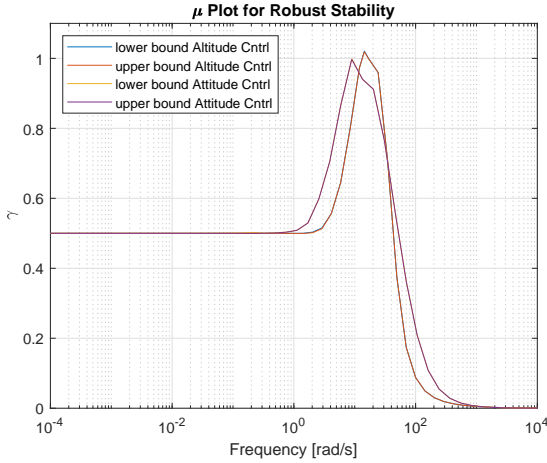|	lower bound	upper bound
Altitude Controller	0.97966	0.98165
Attitude Controller	1.00184	1.00387

Fig. 5. Robust Stability Margins

Fig. 6. μ Plot for Robust Stability

uncertainties. Additionally it also stabilizes the plant for a small amount of uncertainties greater than the specified ones. In contrast to that, the altitude controller is not stabilizing for all defined uncertainties. Nevertheless, these results are interpreted as good enough for the simulation studies. In figure 6 the μ plot for robust stability for each controller is visualized. Both lead to the conclusion, that the closed loop system has very good stability margins for a broad range of frequencies. However, a peaking is introduced around $11\frac{rad}{s}$ respectively $9\frac{rad}{s}$, which leads to the given maximum values of the lower and upper bounds.

B. Simulation Study

For comparing NHC and RC following test cases are proposed:

1) Ext 1: nominal plant (no uncertainties, no disturbances and no noise on measurements)
2) Ext 2: uncertainties in plant
3) Ext 3: uncertainties in plant and noise on measurements
4) Ext 4: uncertainties in plant, noise on measurements and external inputs as described above

Both controller are evaluated from two different points of view

1) The performance is evaluated by the rms (root-mean-squared) value of the errors of the position and yaw angle.
2) Additionally, the controllers are compared regarding a comfort point of view. Thereby the rms values of $\dot{u}$, ω and $\ddot{p}$ are analysed.

All results are visualized in the tables 11, 12, 13, 14 and 15. Obviously, the NHC is better than the RC for the nominal system. For *Ext 2* and *Ext 3* the NHC and the RC behave very similar. No major differences can be observed. However, the RC has the advantage, that noise on the inputs u is reduced by a factor of 10. For all other measures, it can be summarized that each controller performs very well: one has slight advantages in certain areas, while the other has slight advantages in other areas. Nevertheless, the major advantages of the RC are emphasized in *Ext 4*. The additional external inputs lead to huge problems of the NHC, while the performance of the RC does not change significantly. This behavior is also visualized in figures 16, 17, 18 and 19. The NHC lost nearly all of it's performance, but it is still a stable control structure.

V. CONCLUSION AND OUTLOOK

This paper proposes a robust controller structure for a MAV. The introduced results are very promising and emphasize the mightness of robust control theory. The used structure can easily be extended to further performance channels, e.g. use also the transfer functions from reference values to controller outputs as performance channel. The designed robust controller can easily compete with the performance of the NHC for the nominal system. Fortunately, uncertainties, noise and external inputs do not significantly degrade performance. Additionally, using the robust controller specific stability guarantees can be given.

For a future work, the proposed linear structure of the x and y position controller can be integrated into the control structure. Therefore, it will be possible to explicitly handle noise and external inputs on these channels. Additionally, finding performance weights for a suitable solution is very tough. Using more channels, the procedure of determining those weights gets even more difficult. Nevertheless, the used performance requirements must be evaluated in a real-life context, so that the controller can be applied to a MAV in a real environment.

REFERENCES

[1] Bosch Sensortec GmbH. *Small, low power inertial measurement unit*, 10 2018. Rev. 0.9.
[2] Prof. Dr.-Ing. Dr. h. c. O. Sawodny. Handouts of the course "flat systems". Lecture Notes, 2018.
[3] C. W. Scherer. Theory of robust control. Lecture Notes, 2018.
[4] Inc. The MathWorks. robstab - robust stability of uncertain system, 2019. https://de.mathworks.com/help/robust/ref/robstab.html\#bveh4hp-1-wcu, visited 2019-03-01.
[5] u-blox AG. *u-blox 8 GNSS modules*, 7 2016. Rev. 03.
[6] Dr.-Ing. Burak Yüksel. Introduction to aerial robotics. Lecture Notes, 2018.

A. Proof of Theorem 1

Formal proof by contradiction: For a single Δ, it is not possible to identify that it is destabilizing without scanning the right-half plane. However, because Δ is star-shaped, one can choose all uncertainties $\tau\Delta$ obtained by varying $\tau \in [0, 1]$. For $\tau = 1$, $\det(I - M(s)[\tau\Delta(s)])$ has a zero s_1 in $\mathbb{C}^+$. For τ close to zero, the system is stable, because the nominal system is stable. Therefore, if τ decreases from 1 to 0, the unstable zero s_1 moves from $\mathbb{C}^+$ to $\mathbb{C}^-$, because zeros move continuously [3]. Hence, s_1 must hit the imaginary axis for some parameter τ_0 at $i\omega_0$. So $\tau_0\Delta(s)$ is an uncertainty that is still contained in Δ (star-shapeness!) and for which $I - M[\tau_0\Delta]$ has a zero at $i\omega_0$.

B. Small-Gain Theorem

Using theorem 1, the well-known *Small-Gain Theorem* can be derived, which has one big disadvantage: it does not keep in mind the structure of the uncertainty. Assume $\|\Delta\|_\infty < \frac{1}{\gamma}$ following correlation results from theorem 1

$$\det(I - M\Delta) \neq 0$$
$$\Rightarrow 1 \notin \lambda(M(i\omega)\Delta)$$
$$\Rightarrow \rho(M(i\omega)\Delta) < 1$$
$$\Rightarrow \|M(i\omega)\Delta\| < 1 \qquad (13)$$
$$\Rightarrow \|M(i\omega)\|\|\Delta\| < 1$$
$$\Rightarrow \|M(i\omega)\| \leq \frac{1}{\|\Delta\|} = \gamma$$

whereby $\lambda(\cdot)$ are the eigenvalues, and $\rho(\cdot)$ is the spectral radius of $M(i\omega)\Delta$. Obviously, equation (13) points out huge conservativeness of the *Small-Gain Theorem* compared to theorem 1.

C. Structured Singular Value (SSV)

Theorem 2: The structured singular value (SSV) of the matrix M_c with respect to the set Δ is defined as

$$\mu_\Delta(M_c) = \gamma_* =$$
$$\frac{1}{\sup\{\frac{1}{\gamma} \mid \det(I - M_c\Delta) \neq 0 \ \forall\Delta \in \Delta, \ \|\Delta\| < \frac{1}{\gamma}\}}. \qquad (14)$$

Via the scaling factor γ, the set $\gamma^{-1}\Delta$ is inflated or shrinked. For big γ, $I - M_c\Delta$ will be non-singular for any $\Delta \in \gamma^{-1}\Delta$. If γ decreases, it is possible to find some Δ for which $I - M_c\Delta$ will turn out singular. γ_* is the finite critical value for which non-singularity for the set $\gamma^{-1}\Delta$ if γ is greater than γ_* can be assured. This is the reason why γ_* is called non-singularity margin [3].

D. Outlook Robust Control Theory

Using Linear Matrix Inequalities (LMI) techniques, it is possible to extend the given results into a more general framework [3]. However, this serves more as an outlook, and is not used in this project paper.

- greater flexibility in choosing the performance specification (e.g. H_2-norm constraints (stochastic noise reduction), amplitude constraints)
- possibility to include time-varying parametric, non-linear static and nonlinear dynamic uncertainties in the robustness test
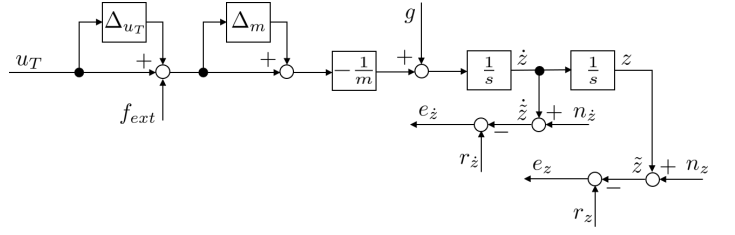- systematic design of gain-scheduling controllers (for certain class of nonlinear control problems)

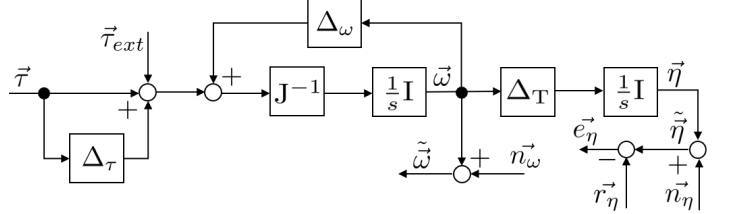Fig. 7. MAV altitude dynamic model with uncertainties.

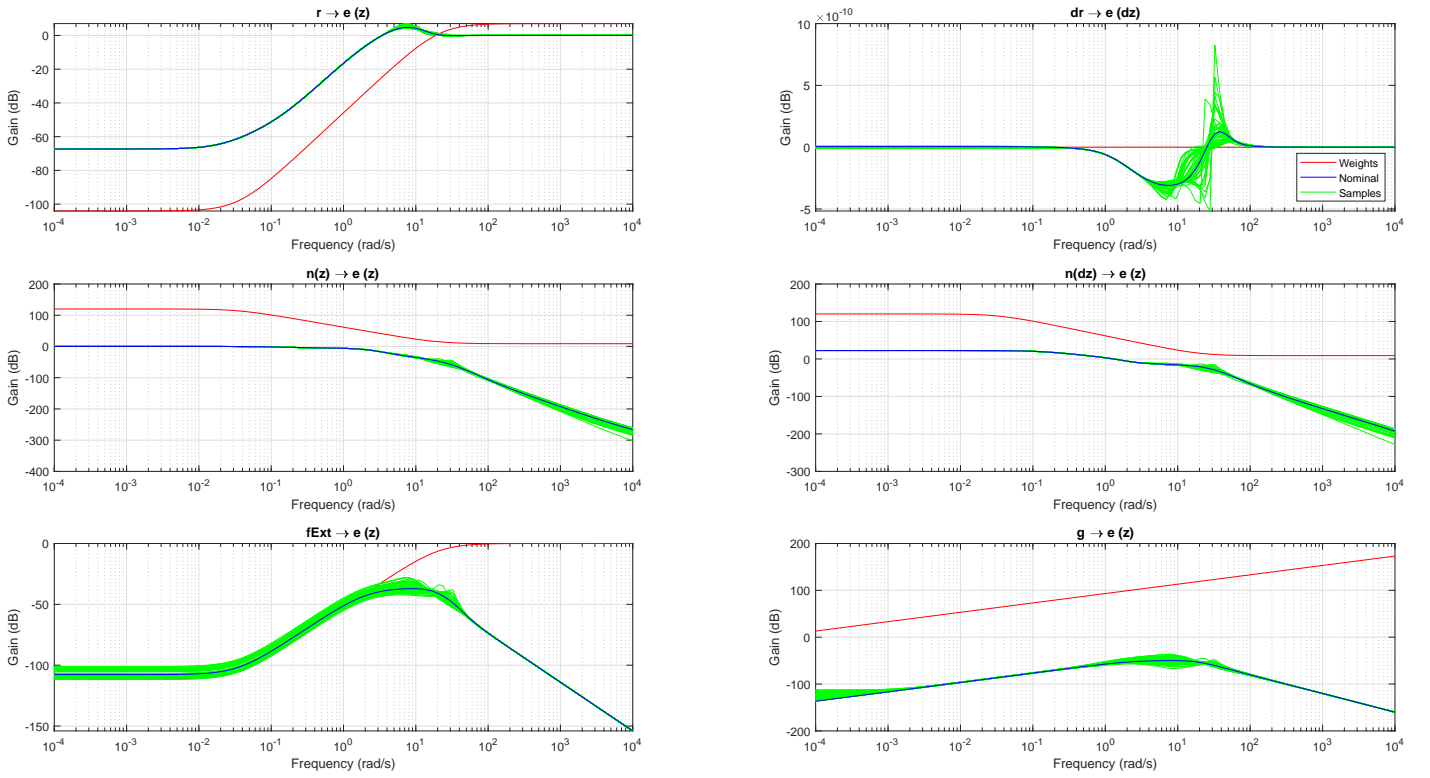Fig. 8. MAV rotational dynamic model with uncertainties.

Fig. 9.   Bode Plot of Altitude Controller

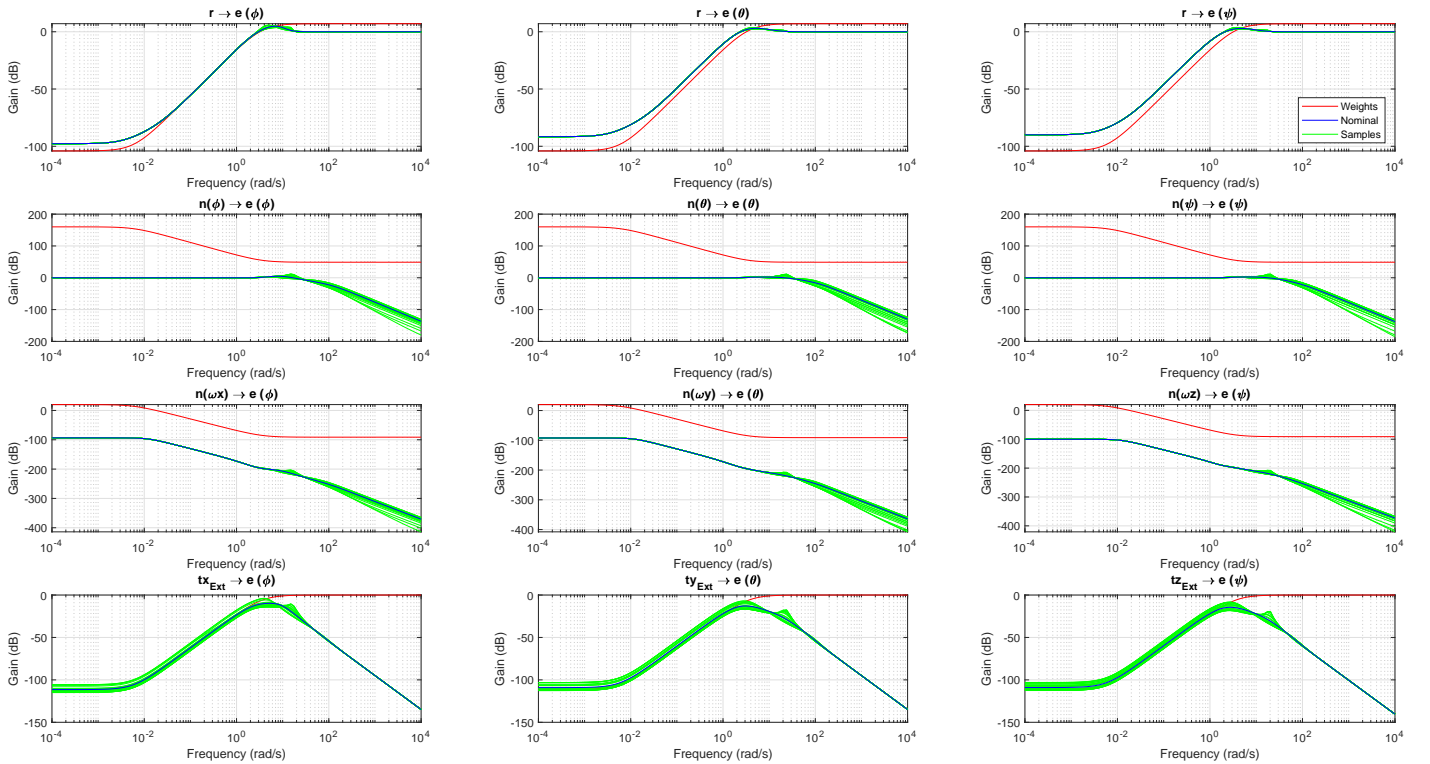Fig. 10.   Bode Plot of Attitude Controller

SIMULATION RESULTS

Cntrl	Ext	$RMS(e_x)$	$RMS(e_y)$	$RMS(e_z)$	$RMS(e_\psi)$
NHC	1	0.04806	0.03223	0.00673	0.09777
RC	1	0.03899	0.02146	0.03194	0.10077
NHC	2	0.03844	0.02463	0.09458	0.09633
RC	2	0.05927	0.04036	0.03194	0.10021
NHC	3	0.03209	0.02024	0.32773	0.09635
RC	3	0.06712	0.04502	0.13350	0.10015
NHC	4	0.39650	0.32433	0.51697	0.21135
RC	4	0.06687	0.04572	0.13333	0.10016

Fig. 11.   Simulation Study - Comparison NHC with Robust Controller - Control Error

Cntrl	Ext	$RMS(u_T)$	$RMS(\tau_x)$	$RMS(\tau_y)$	$RMS(\tau_z)$
NHC	1	4.90591	0.00460	0.00903	0.05018
RC	1	4.90602	0.00154	0.00182	0.05872
NHC	2	3.59854	0.00661	0.01526	0.04371
RC	2	3.59818	0.00231	0.00372	0.04713
NHC	3	3.99734	0.12254	0.24688	0.04585
RC	3	3.72953	0.13043	0.23695	0.19433
NHC	4	4.05909	1.05102	1.30903	0.58060
RC	4	3.75824	0.66631	0.98726	0.58583

Fig. 12.   Simulation Study - Comparison NHC with Robust Controller - u

Cntrl	Ext	$RMS(\dot{u}_T)$	$RMS(\dot{\tau}_x)$	$RMS(\dot{\tau}_y)$	$RMS(\dot{\tau}_z)$
NHC	1	0.02229	0.09790	0.19265	0.32973
RC	1	1.85078	0.02968	0.05223	0.25096
NHC	2	0.17702	0.10920	0.18657	0.38113
RC	2	2.14128	0.03295	0.05645	0.29197
NHC	3	254.38797	3696.78744	3696.48458	53.69564
RC	3	26.86262	12.50864	25.31862	13.63255
NHC	4	257.52272	1512.71386	1508.57635	236.68005
RC	4	26.85987	12.42331	25.16268	13.59044

Fig. 13.   Simulation Study - Comparison NHC with Robust Controller - $\dot{u}$

Cntrl	Ext	$RMS(\omega_x)$	$RMS(\omega_y)$	$RMS(\omega_z)$
NHC	1	0.01150	0.02213	0.28939
RC	1	0.00670	0.00894	0.34270
NHC	2	0.01451	0.02943	0.28890
RC	2	0.00957	0.01271	0.34079
NHC	3	0.05266	0.11901	0.28883
RC	3	0.08046	0.07840	0.34604
NHC	4	0.51204	0.49167	0.31553
RC	4	0.08091	0.07943	0.34605

Fig. 14.   Simulation Study - Comparison NHC with Robust Controller - ω

Cntrl	Ext	$RMS(\ddot{p}_x)$	$RMS(\ddot{p}_y)$	$RMS(\ddot{p}_z)$
NHC	1	0.08249	0.16200	0.47786
RC	1	0.02653	0.03189	0.55921
NHC	2	0.09947	0.17105	0.52084
RC	2	0.04196	0.04704	0.56922
NHC	3	0.97717	1.71335	0.53157
RC	3	1.44247	1.66086	1.49492
NHC	4	9.57602	7.51734	1.58573
RC	4	1.44279	1.66281	1.49497

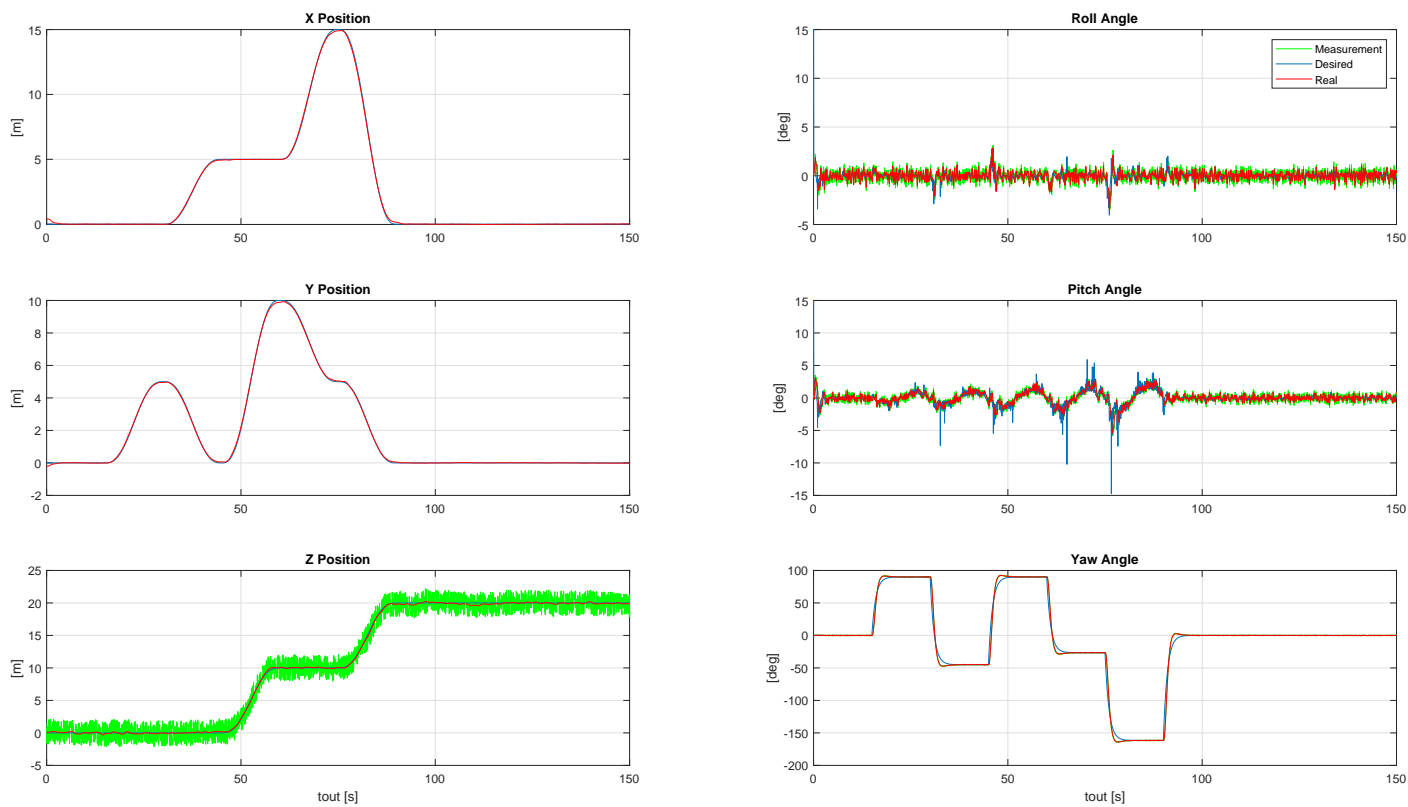Fig. 15.   Simulation Study - Comparison NHC with Robust Controller - $\ddot{p}$

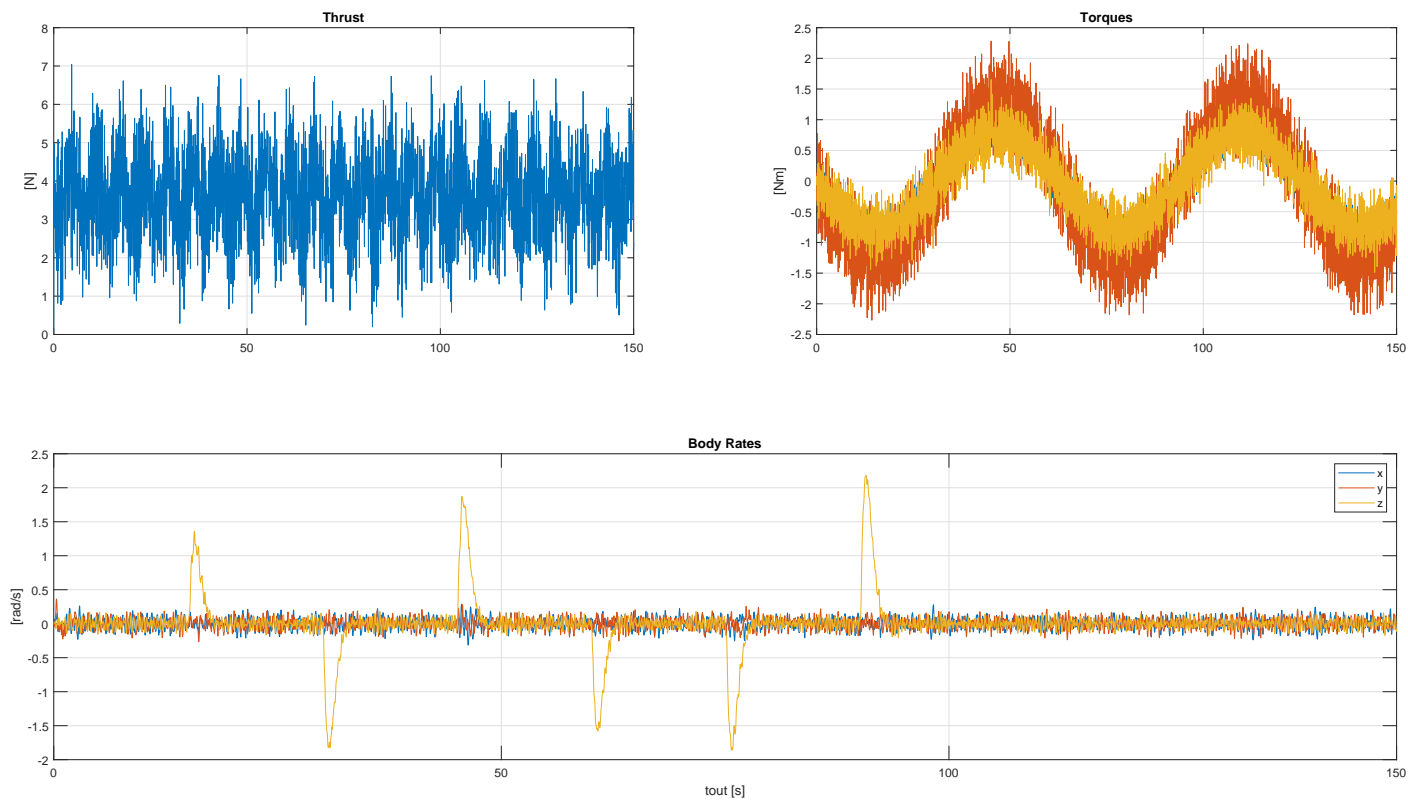Fig. 16.   Simulation Results: Robust Controller

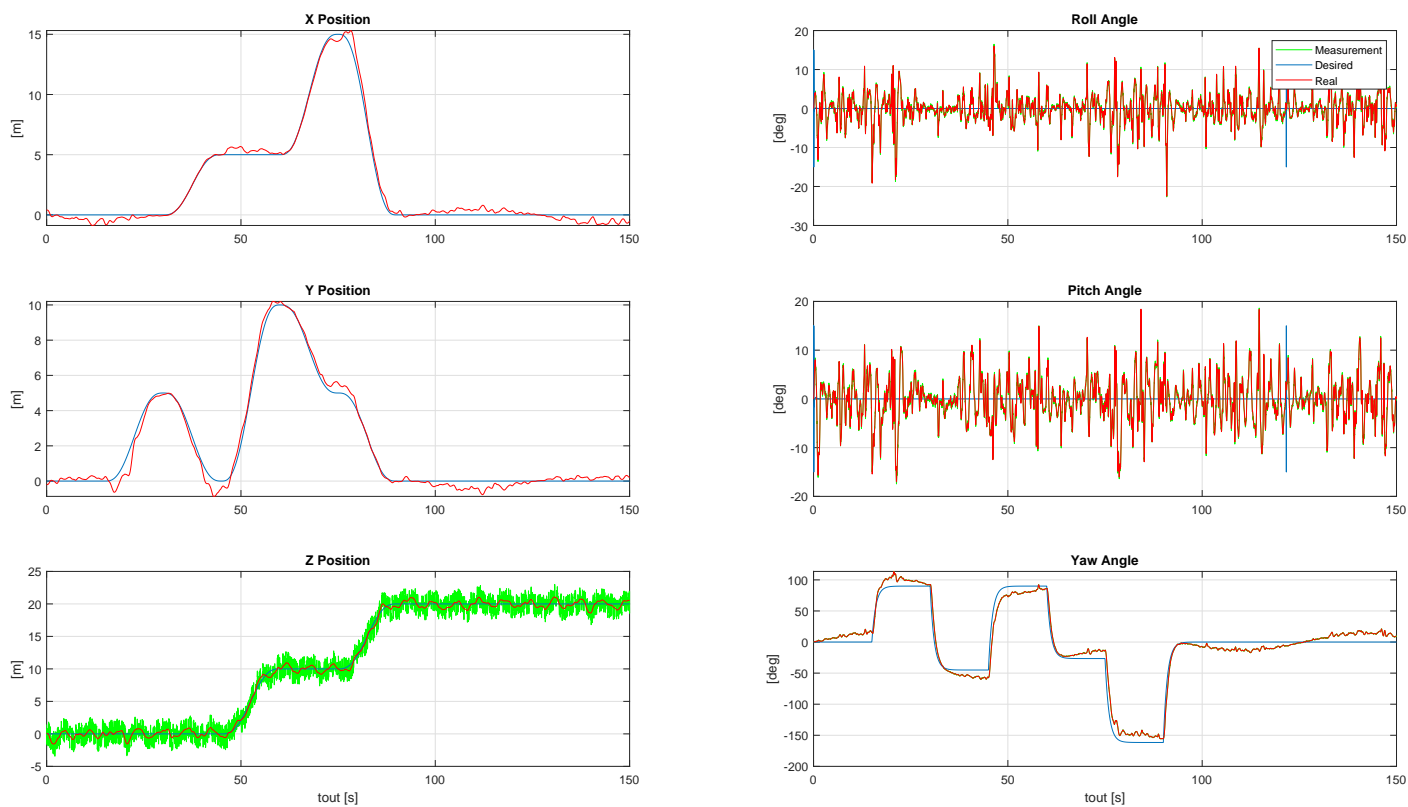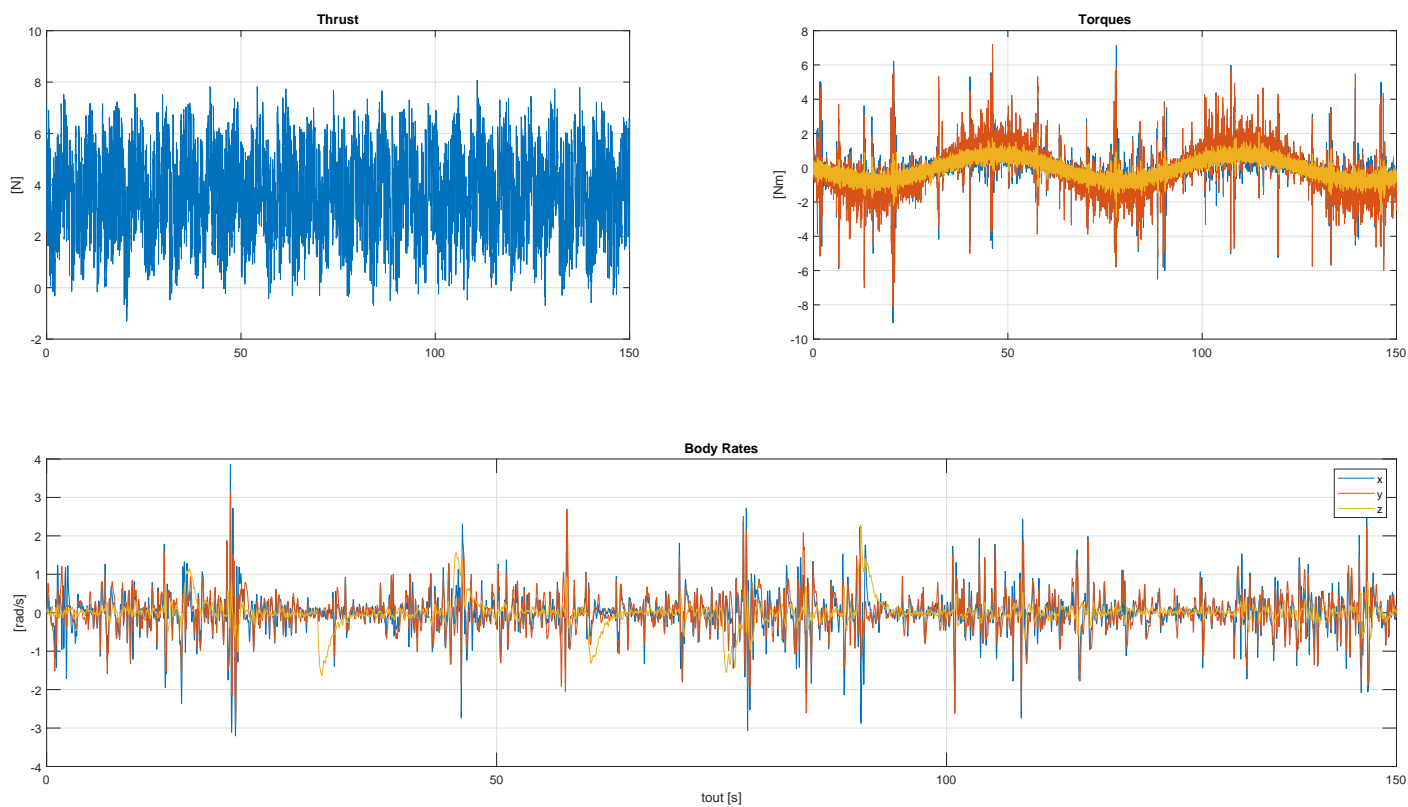Fig. 17.   Simulation Results: Robust Controller - Inputs

Fig. 18.   Simulation Results: NHC

Fig. 19.   Simulation Results: NHC - Inputs